Journal of Nuclear Materials 380 (2008) 30–45

Contents lists available at ScienceDirect

Journal of Nuclear Materials

journal homepage: www.elsevier.com/locate/jnucmat

Zircaloy-4 and M5® high temperature oxidation and nitriding in air

C. Duriez [a,*], T. Dupont [b], B. Schmet [b], F. Enoch [b]

[a] Institut de Radioprotection et Sûreté Nucléaire, Direction de Prévention des Accidents Majeurs, Centre de Cadarache, 13115 St Paul Lez Durance, France
[b] Université Technologique de Troyes, BP 2060, 10010 Troyes, France

ARTICLE INFO

Article history:
Received 11 September 2007
Accepted 10 July 2008

PACS:
28.52.Fa
28.52.Nh
81.05.Bx
82.20.Pm

ABSTRACT

For the purpose of nuclear power plant severe accident analysis, degradation of Zircaloy-4 and M5® cladding tubes in air at high temperature was investigated by thermo-gravimetric analysis, in isothermal conditions, in a 600–1200 °C temperature range. Alloys were investigated either in a 'as received' bare state, or after steam pre-oxidation at 500 °C to simulate in-reactor corrosion. At the beginning of air exposure, the oxidation rate obeys a parabolic law, characteristic of solid-state diffusion limited regime. Parabolic rate constants compare, for Zircaloy-4 as well as for M5®, with recently assessed correlations for high temperature Zircaloy-4 steam-oxidation. A thick layer of dense protective zirconia having a columnar structure forms during this diffusion-limited regime. Then, a kinetic transition (breakaway type) occurs, due to radial cracking along the columnar grain boundaries of this protective dense oxide scale. The breakaway is observed for a scale thickness that strongly increases with temperature. At the lowest temperatures, the M5® alloy appears to be breakaway-resistant, showing a delayed transition compared to Zircaloy-4. However, for both alloys, a pre-existing corrosion scale favours the transition, which occurs much earlier. The post transition kinetic regime is linear only for the lowest temperatures investigated. From 800 °C, a continuously accelerated regime is observed and is associated with formation of a strongly porous non-protective oxide. A mechanism of nitrogen-assisted oxide growth, involving formation and re-oxidation of ZrN particles, as well as nitrogen associated zirconia phase transformations, is proposed to be responsible for this accelerated degradation.

1. Introduction

In the field of nuclear plant safety analysis, various low probable accidental situations may result in fuel rod exposure to air-containing atmospheres. Major examples are spent fuel storage pond loss of water accident and reactor pressure vessel breaching following a thermal shock event. Air ingress under shutdown conditions, when the reactor coolant system is opened to the containment atmosphere, may also occur. Even if such situations are of very low probability, they potentially have severe consequences. The degradation of the fuel cladding upon air exposure up to its failure will have direct implications on the source term (inventory of radio-nuclides released in the environment). The prediction of this degradation requires, amongst others, an understanding of the oxidation behaviour of zirconium alloys when exposed to air at high temperatures. In comparison with steam, the presence of air is expected to result in a more rapid escalation of the accident, mainly because (i) the $Zr + O_2$ reaction enthalpy (−1100 KJ/mol at 298 K) is about 80% higher than that of the $Zr + H_2O$ reaction (−616 KJ/mol at 298 K), (ii) due to the presence of nitrogen, the zirconium alloys degradation is much faster in air than in steam.

Oxidation of zirconium alloys at high temperature for severe accident analysis has been widely studied in steam, however, the existing data regarding air oxidation in the temperature range of interest are scarce. Evans and co-workers have early demonstrated with pure zirconium that the oxidation process above 1050 °C is strongly influenced by the simultaneous presence of oxygen and nitrogen [1]. Later on, the work conducted at FZK by Leistikow and Berg with Zircaloy-4 samples in the 750–1250 °C temperature range has shown that the influence of nitrogen is predominant at even lower temperature for alloyed zirconium [2]. However, the exact role of zirconium nitride on the cladding degradation process is poorly understood. It remains unclear to which extent the nitrogen effect is responsible for the kinetic acceleration of the oxidation process that has been observed by these authors.

Further, it should be stressed that most of the existing data have been obtained with bare samples. The effect of the pre-existing corrosion scale on further air oxidation of the cladding has been addressed only recently at Argonne National Laboratory [3].

For the M5®([1]) French niobium based alloy, there is no published air oxidation data in the open literature.

* Corresponding author. Tel.: +33 4 42 19 95 05; fax: +33 4 42 19 91 62.
E-mail address: christian.duriez@irsn.fr (C. Duriez).

[1] (*) M5® is a registered trademark of AREVA NP.

0022-3115/$ - see front matter © 2008 Elsevier B.V. All rights reserved.
doi:10.1016/j.jnucmat.2008.07.002

Table 1
Chemical composition of the investigated alloys

Alloy	Sn (wt%)	Nb (wt%)	Fe (wt%)	Cr (wt%)	S (ppm)	O (wt%)	C (ppm)	H (ppm)
Zircaloy-4	1.45–1.48	<50 ppm	0.21	0.10		0.123–0.129	133–140	3–8
M5®	<30 ppm	1.00	0.03	40 ppm	14–18	0.139–0.149	20–26	⩽4

A new experimental program has therefore been launched at the French Institute of Radioprotection and Nuclear Safety (IRSN). Centimetre size samples were cut from French PWR geometry Zircaloy-4 and M5® cladding tubes. Double side oxidation tests have been performed by thermogravimetric analysis (TGA) to generate detailed kinetic data. The 600–1200 °C temperature range has been investigated, where, due to the high enthalpy of the $Zr + O_2$ reaction, rapid temperature escalation of the fuel assemblies is expected in accidental situation. Synthetic dry air was used as the oxidant media. Samples are studied either in the 'as received' bare state, or after pre-oxidation in steam, to simulate the effect of in-reactor corrosion. An extensive kinetic database has been produced. This paper presents illustrative examples of data. The results are discussed with the help of post-test metallographic inspections. Clarifications on the mechanism of the accelerated degradation upon the influence of nitriding are proposed.

2. Experimental

2.1. Sample preparation

The samples are cladding tube segments, cut by machining from standard French PWR cladding provided by Areva NP (Inner diameter 8.4 mm, Outer diameter 9.53 mm). Composition of the 2 alloys is given in Table 1. Most of the tests have been performed with 20 mm long segments, but some have been cut to a 10 or 7 mm length. The bare samples are cleaned in acetone, then rinsed in ethanol and dried. Their initial mass is measured with a 1 mg accuracy.

2.1.1. Pre-oxidation

To simulate a pre-existing in-reactor corrosion scale, samples have been pre-oxidised in steam at 500 °C. The choice of the pre-oxidation temperature results from a compromise between the representativeness, the cost and the duration of the pre-oxidation. The pre-oxidation experimental device consists of a steam generator and a tubular resistive vertical furnace. Fifteen samples (20 mm high cladding segments) are placed on a 3-level sample holder inside a 45 mm diameter Inconel® tube.

The steam generator delivers argon + steam mixture. The steam mass flow rate is set to 40 g/h and a 1 L/mn Ar volumic flow rate is used, leading to a 0.45/0.65 steam/Ar volumic ratio. The mixture is injected from the top and flows down in the Inconel® tube. The lower end of the tube is opened and thus the pre-oxidation takes place at atmospheric pressure.

Zircaloy-4 and M5® batches have been pre-oxidised during 20 days. For Zircaloy-4, 60 days pre-oxidation batches have also been prepared to simulate high burn-up spent fuel cladding. Samples are further referred as 20d-PO (20 days pre-oxidised) and 60d-PO. The mean oxide scale thickness is calculated from the mass gain assuming dense zirconia. The contribution of absorbed hydrogen to the mass gain is taken into account considering an hydrogen pick-up fraction of 75% for Zircaloy-4 and 15% for M5® (see the justification in next section) For samples selected for further TGA air oxidation tests, the mean oxide scale thickness were in the range: 15.2–17.8 μm for the 20d-PO Zircaloy-4, 58.9–81.8 μm for the 60d-PO Zircaloy-4 and 8.7–17.8 μm for the 20d-PO M5®.

One pre-oxidised sample from each batch was used for metallographic examination. Typical optical micrographies are given in Fig. 1. Thickness measurements on the metallographies show that, for a given cut, the scale is homogeneous on the circumference within ±20% (not including the variations due to the short range waviness of the metal/oxide interface observed for Zircaloy-4). At high magnification the αZr(O) metallic layer, revealed by the mechano-chemical polishing step, can be seen at the metal–oxide interface. Its thickness is within 1–2 μm for Zircaloy-4 as well as for M5®.

For both alloys, V-shape, regularly spaced radial cracks, not penetrating down to the metal, are visible in the oxide on the metallographic cuts (Fig. 1). They form a network of cracks that gives to the sample surface a 'snake skin' aspect. Because of their V-shape, they are believed to be due to sample growth, by metal creep upon the tensile stress field applied by the growing oxide layer, favoured by the rather elevated temperature used to keep reasonable pre-oxidation times.

Metallographies also show that, for Zircaloy-4, these 'corrosion' scales grown in steam at 500 °C exhibit a stratified structure defined by a periodic network of circumferential cracks. The thickness of the surface top layer is measured to be around 3–5 μm, while the subsequent layers, clearly thicker, have a mean thickness of about 6–7 μm. Such periodic features are commonly observed on Zircaloy-4 after autoclave corrosion in PWR conditions, but with a periodicity of the order of 2 μm [4,5]. The same kind of layering is also reported for corrosion scales grown under irradiation in PWR reactors, but with a layer thickness in the 5–10 μm range [6], comparable to what we have obtained under steam at 500 °C. Detailed investigations by transmission electron microscopy [4] and Raman spectroscopy [7] have shown that complex microstructural considerations should be taken into account to explain the periodic radial fissuring of the zirconia. Yilmazbayhan and co-workers have proposed that the circumferential fissuring is favoured by the presence of a zone of equiaxed small grains enriched in the tetragonal phase [4]. Relaxation of the compressive stress field also plays a role. A mechanism of relaxation by buckling has been put forward to describe the spallation and cracking of NiO oxidation scales submitted to an externally applied compressive stress [8], or also in the case of spallation of an Al_2O_3 oxidation layer (on a

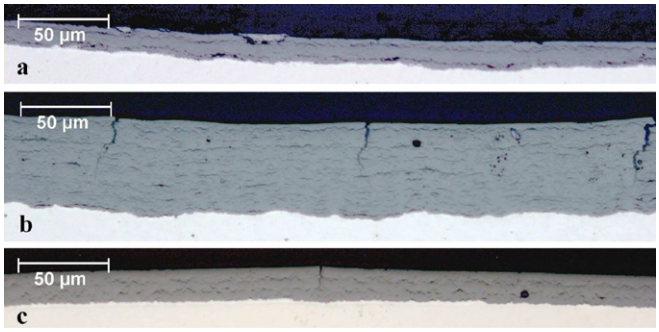

Fig. 1. Optical metallographies of claddings pre-oxidised in steam at 500 °C. (a) Zry-4, 20-days pre-ox., oxide thickness = 16 μm. (b) Zry-4, 60-days pre-ox., oxide thickness = 50 μm. (c) M5®, 20-days pre-ox., oxide thickness = 14 μm.

NiCrAlY substrate) submitted to a compressive stress upon cooling [9]. Such a buckling mechanism, under the influence of the high compressive stresses that develop into the growing oxide, can play a role in the circumferential cracking observed for Zr alloys corrosion scales. It would give way to the periodic detachment of the last grown layer for a given thickness and would result in the observed stratified structure. The periodicity of the process would be high if part of the compressive stresses can be relaxed by sample growing. Irradiation induced growing then may explain why the layer thickness is higher for in pile corrosion in comparison to autoclave corrosion. In other respects, thermal creep growing can explain the high layer thickness that we observe at 500 °C. Whatever, from this point of view, our 'corrosion' scales are representative of the in-pile PWR corrosion.

For M5®, circumferential cracks are also present, but they are less numerous, the oxide scales appear more compact. Nevertheless, the thickest pre-oxidation scales generally exhibit the layered structure. The layer thickness is in the 5–7 μm range (Fig. 1(c)).

2.1.2. Hydrogen content

When questioning about the ability of steam oxidation to simulate in-reactor cladding corrosion, the question of hydrogen dissolution in the cladding also has to be addressed. Mean hydrogen concentrations of about 600 ppm are usually reached for end of life Zircaloy-4 cladding. Moreover, hydrogen accumulation occurs close to the metal oxide interface in a 10–20 μm deep rim, where concentrations as high as 1600 ppm are found. It has been shown by autoclave tests that such high hydrogen concentrations contribute to increase the low temperature Zircaloy corrosion rate [10]. However, in accidental situation at high temperature, the dissolved hydrogen will rapidly redistribute and the high concentration rim will disappear. The effect of uniformly dissolved hydrogen on air oxidation kinetics of zirconium alloys has been addressed recently by ANL [11]. Only the Westinghouse Zirlo alloy has been investigated. The cladding samples were hydrogen loaded by gaseous diffusion at 320 °C up to concentrations in the 100–1000 ppm range. The air oxidation of these hydrided samples was investigated in a 300–600 °C temperature range. It was concluded that the difference with 'as received' Zirlo was not significant.

After steam pre-oxidation at 500 °C, we have measured on few samples the hydrogen content by the fusion technique. For Zircaloy-4, very high values have been obtained (see Table 2). The hydrogen uptake fraction calculated from these measurements is about 0.75 for the Zircaloy-4 alloy and 0.12–0.15 for M5®. After chemical attack, metallographies exhibit for the M5® samples a uniform distribution of precipitated hydride filaments (Fig. 2). With the Zircaloy-4 samples, the chemical attack leads to uniformly frosted surfaces, likely because of a very high density of hydride precipitates. When performing air oxidation tests at high temperature, it is thought that part of the high amount of hydrogen is released back by the metal during the heat-up phase under argon. Moreover, referring to the ANL study [11], it will be considered here that the effect of dissolved hydrogen on air oxidation is of second order compared to the effect of a pre-existing corrosion scale. The hydrogen effect will be investigated separately with Zircaloy-4 and M5® in a subsequent campaign of TGA experiments.

Table 2
Hydrogen content in the metal after pre-oxidation in steam at 500 °C, measured by the fusion method

Alloy	Sample	Pre-oxidation duration (days)	Scale thickness (μm)	H content (wppm)	H pickup fraction
Zircaloy-4	1	20	15.3	1160	0.74
	2	20	17.4	1360	0.74
	4	60	64.3	5270	0.70
	5	60	49.2	4190	0.70
M5®	5	20	11.2	180	0.16
	6	20	13.1	165	0.12

Fig. 2. Optical metallography of a M5® sample pre-oxidised in steam at 500 °C during 20 days, after chemical attack for revelation of hydride precipitates.

2.1.3. Metal microstructural changes during pre-oxidation

The Zircaloy-4 cladding tube material is known to have a textured microstructure, with grains strongly elongated in the axial direction of the tube, given by the cold rolling process. For stress-relieved Zircaloy-4, the tubes are annealed at 460 °C, temperature at which the grain microstructure does not evolve within the annealing time. An annealing temperature of 580 °C is used when recrystallized Zircaloy-4 is needed (guide tube, grid, ...). The temperature of 500 °C at which we proceed to the steam pre-oxidation is lower than this recrystallisation temperature. However, because of the long annealing duration at 500 °C, grain growth may occur. Nevertheless, this aspect was not investigated. It is considered that the metallurgical transformation during the pre-oxidation is of minor importance, taking into account that the samples are further heated at much higher temperature for the subsequent air oxidation tests.

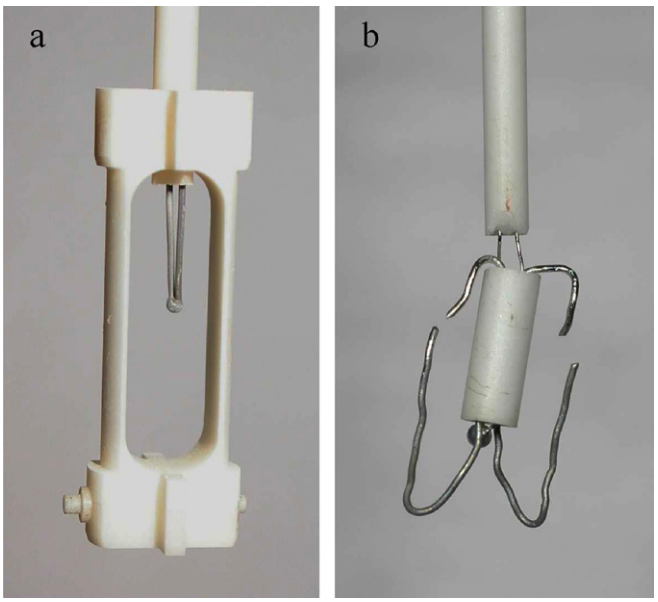

Fig. 3. Sample holders (a) Alumina, for 20 mm open cladding segments, with thermocouple. (b) Pt wires, used with short samples for better access of air to the sample inner surface, with thermocouple.

2.2. Thermogravimetric apparatus

The thermogravimetric analyser (TGA) is a SETARAM single furnace thermobalance. The furnace chamber is a vertical alumina tube, 17 mm ID. The temperature is regulated through a Pt–6%Rh/Pt–30%Rh thermocouple located close underneath the sample. The temperature homogeneity at the centre of the heating zone has been measured to be within 3 °C over a 20 mm height at 1000 °C and low gas flow rate. A specific alumina sample holder has been designed, which comprises a second Pt–6%Rh/Pt–30%Rh thermocouple that measures the temperature very close (about 0.5 mm) to the sample inner surface (Fig. 3(a)). Two mass flow meters control the gas flows in the furnace. Isothermal oxidation tests are performed using a computer controlled sequence: heat-up at 20 K/mn under 500 mL/mn argon, 10 mn stabilisation at the desired temperature under argon, then switch to dry synthetic air. Most of the time, high air flow rates (500 or 1000 mL/mn) are used to limit the sample temperature elevation resulting from fast oxidation of the bare metal at the air admission, and to provide sufficient oxygen supply. Blank tests have shown that such high flow rates induce a significant fluctuation (few milligrams) of the TG signal when switching from argon to air. However, it is only a short transient perturbation and blank subtraction is not needed. The oxidation test is stopped after a given duration or when a given mass increase is reached, by switching back to argon and shutdown of the furnace power.

3. Tests grids

Tables 3–6 give the test conditions of the TGA experiments for the 'as received' bare Zircaloy-4, the steam-pre-oxidised Zircaloy-4, the 'as received' bare M5® and the steam-pre-oxidised M5®, respectively. Equivalent cladding reacted (ECR) is calculated as the ratio of the mass gained at the end of the test, determined by post-test off-line weighting, to the total reachable mass gain, if all Zr is transformed into stoichiometric zirconia). For pre-oxidised samples, it includes (total ECR) or not (air ECR) the mass gained during the pre-oxidation in steam.

3.1. Bare Zircaloy-4 (Table 3)

With the bare 'as-received' Zircaloy-4, the experiments were first continued up to total oxidation, to get kinetic data for the whole degradation process, and repeated at least once to check

Table 3
Test grid for 'as-received' bare Zircaloy-4

Furnace temp. (°C)	Sample length (mm)	Air flow rate (mL/mn)	Air exposure duration	ECR (%)	Peak temp. elevation (°C)	Time to transition (min)	ZrO_2 thickness at transition (μm)
600	20	500	240 h	34.9	0.5	442	4.0
	20	50	278 h	45.2	0.5	433	4.2
	20	500	118 h	13.7	0.75	507	4.8
700	20	500	60 h	84.4	3.7	113	7.2
	20	500	59.5 h	82.7	5.7	94	7.1
	20	500	15 h	16.8	7.9	86	6.9
800	20	500	17 h	97.6	20.5	29	10.7
	20	500	12.5 h	98.2	21.2	26	9.9
	20	500	200 min	16.4	23.9	34.7	11.1
	7	500	13.3 h	99.7	[b]	19.2	11.1
850	20	500	260 min	98.1	26.3	18.1	15.0
	20	500	220 min	72.6	28.6	19.2	14.9
	20	500	190 min	59.6	24.2	21.6	15.5
	20	500	90 min	13.6	30.8	16.1	14.2
	7	500	260 min	72.1	14.5	11.2	14.4
900	20	500	260 min	⩾85	46.7	20.1	23.7
	20	500	220 min	⩾86	43.9	19.0	23.1
	20	500	110 min	18.7	47.1	20	23.6
	20	500	100 min	16.2	47.1	20.2	23.3
	7	500	180 min	71	47.0	16	25.7
	7	500	190 min	73.2	35.0	20	28.2
950	20	500	283 min	⩾86	78.6	19.9	36.6
	20	500	200 min	⩾93	63.6	18.2	34.0
	20	500	55 min	17.3	88.0	17.5	35.0
	7	500	146 min	98	76.0	18.2	39.3
	7	500	70 min	26	86.0	19.9	40.7
1000	20	500	168 min	⩾88	125	17.2	79.4
	20	500	101 min	⩾92	128	14.2	82.2
	20	500	101 min	⩾93	115	14.8	80.4
	20	500	17 min	16.4	[b]	[c]	[c]
	20	500	17 min	23.5	178	[c]	[c]
	7[a]	1000	85 min	95.2	137	16.1	64.5
	7[a]	1000	103 min	78	253	12.3	80.6
1100	20	500	14 min	70.4	209	No breakaway transition at 1100 °C	
	20	500	17 min	70.5	187		
	7	1000	50 min	54.9	221		
	7	1000	120 min	97.8	194		
	7[a]	1000	60 min	58.6	232		
1200	20	500	7 min	69.1	210	No breakaway transition at 1200 °C	
	7	1000	8.5 min	55.8	260		
	7[a]	1000	15 min	67.2	255		

ECR = Equivalent cladding reacted.
[a] Test performed with the modified sample holder.
[b] Temperature measurement failed.
[c] Test was stopped before the transition.

Table 4
Test grid for steam pre-oxidised Zircaloy-4

Furnace temp. (°C)	Sample length (mm)	Pre-ox. scale thickness (μm)	Air flow rate (mL/mn)	Air exposure duration	Air ECR (%)	Total ECR (%)
600	20	15.3	50	189 h	24.9	28.7
700	20	15.2	500	21.9 h	27.4	31.2
	20	17.3	500	78.3 h	86	91.2
	10.27	**58.9**	**50**	**71.3 h**	**62.0**	**78.5**
	10.3	**81.8**	**50**	**85.3 h**	**47.7**	**66.2**
800	20	17.8	500	14.1 h	90.4	96.0
	20	15.3	500	17.4 h	95	95.4
	20	15.2	500	6 h	45	46.2
	10.21	**61.0**	**500**	**10 h**	**28.5**	**42.3**
	10.01	**79.9**	**500**	**20.2 h**	**36.5**	**55.0**
850	20	15.9	500	246 min	76.6	81.3
	20	17.1	500	252 min	>90.6	>95.8
	20.12	**61.2**	**500**	**298 min**	**28.2**	**42.1**
	8.63	**60.7**	**500**	**700 min**	**83.9**	**97.7**
900	20	17.1	500	198 min	>71	>75.9
	20	16.6	500	80 min	15.8	20.1
	11.27	**60.7**	**500**	**250 min**	**68.0**	**81.7**
	10.06[a]	**79.8**	**500**	**285 min**	**56.4**	**74.5**
950	20	17.1	500	129 min	91.8	97.3
	10.0	**58.9**	**500**	**104 min**	**70.5**	**83.8**
	9.90	**74.8**	**500**	**70 min**	**36.7**	**53.7**
1000	20	17.2	500	100 min	94.1	98.1
	20	15.0	500	105 min	95.7	100
	10.0	**81.3**	**500**	**73 min**	**69.1**	**87.6**
1100	**9.66**[a]	**79.8**	**1000**	**38 min**	**68.7**	**86.7**
	9.71[a]	**81.8**	**1000**	**60 min**	**55.0**	**73.5**
	9.67[a]	**61.0**	**1000**	**27 min**	**70.1**	**83.9**
1200	**9.6**[a]	**74.2**	**1000**	**33 min**	**69.3**	**86.0**

ECR = Equivalent Cladding Reacted.
[a] Test performed with the modified "more open" sample holder, in bold : 60 days pre-oxidised samples; others: 20 days pre-oxidised samples.

Table 5
Test grid for 'as-received' bare M5®

Furnace temp. (°C)	Air flow rate (mL/min)	Air exposure duration	ECR (%)	Peak temp. elevation (°C)	Time to transition (min)	ZrO_2 thickness at transition (μm)
600	50	278 h	32.6	0.5	2470	16.7
700	500	83.5 h	68	7.5	459	19.0
	500	94 h	87	8.2	451	19.6
800	500	22.5 h	96.4	26.5	92	19.1
	500	13.3 h	39.5	28.3	93	19.3
850	500	260 mn	>26.3	38.5	36.6	19.4
	500	1200 mn	95.7	29.6	39.7	20.4
	500	511 mn	>58.8	43.2	131.6	33.3
	500	339 mn	44.5	37.0	30.93	18.8
900	500	230 mn	58.8	63.3	27.9	24.9
	500	230 mn	48.3	73.3	38.1	27.6
	500	151 mn	28.3	69.3	35.7	26.8
950	500	190 mn	96.8	117.3	23	42.7
	500	110 mn	61.1	120.6	25	50.1
1000	500	190 mn	99.5	166.5	20.0	81.3
	500	130 mn	99.9	162.1	21.2	91.2
	500	39 mn	37.3	163.6	20.7	104

ECR = Equivalent cladding reacted.
All tests are performed with 20 mm long samples.

reproducibility. These long duration tests have been completed by shorter duration ones, specifically dedicated to post-test metallographic preparations. Here, a 15% ECR was targeted to have enough metal left. Most of the tests have used 20 mm-long samples and a 500 mL/mn air flow rate. However, at the highest temperatures, very high oxygen consumption rates were observed, leading to oxygen-starved situations. Thus, the air flow rate was increased to 1000 mL/mn and the sample length was reduces to 7 mm-long samples, resulting in an increase by a factor of 6 of the oxygen flow

Table 6
Test grid for steam pre-oxidised M5®

Furnace temp. (°C)	Pre-ox. scale thickness (μm)	Air flow rate (mL/mn)	Air exposure duration (mn)	Air ECR (%)	Total ECR (%)
700	15.7	500	5225	74.4	79.0
800	17.2	500	940	82.0	86.0
850	17.8	500	159	51.0	55.2
	9.2	500	192	57.9	59.7
900	16.9	500	57.3	78.5	82.5
	16.7	500	49	87.0	90.9
	8.7	500	57	59.3	61.3
950	14.9	500	>60	94.0	97.5
	16.9	500	53.5	86.2	90.0
1000	15.5	500	106	95.9	100
	13.9	500	105	94.0	97.2

ECR = Equivalent cladding reacted.
All tests are performed with 20 mm long samples.

rate per surface unit (O_2FR/S) of exposed metal (i.e. $O_2FR/S = 10$ g s^{-1} m^{-2} to $O_2FR/S = 60$ g s^{-1} m^{-2}). Last, the alumina sample holder was replaced by platinum wires to facilitate the access of air to the inner surface of the tube (Fig. 3(b)). To check a possible influence of the reduced sample size (edge effects), some tests were performed with short samples and a 500 mL/mn air flow rate, at 800, 850, 900 and 950 °C, temperatures at which problems of oxygen starvation are not expected. Here, no significant difference in test results with tests with 20 mm long samples was observed.

3.2. Pre-oxidised Zircaloy-4 (Table 4)

Tests have been first performed with the 20d-PO samples (pre-oxidation scale mean thickness: 15.2–17.8 μm), then with the 60d-PO (pre-oxidation scale mean thickness: 58.9–81.8 μm). The later, pre-oxidised in a 20 mm length, were cut in two pieces before the TGA tests, because the number of samples was limited. At the highest temperatures (1100 and 1200 °C), only 10 mm long, 60d-PO samples and the modified sample holder were used.

3.3. Bare M5® (Table 5)

The M5® test-grids were less extensive than for Zircaloy-4. Only the 600–1000 °C temperature range has been covered. The sample length was always 20 mm. At 850 °C and 900 °C, with the bare samples, most of the tests had to be interrupted prematurely: because of very strong deformations, the samples came in contact with the furnace alumina tube and the TGA signal was lost.

3.4. Pre-oxidised M5® (Table 6)

Because the M5® alloy is known to be more resistant to in-reactor corrosion, only 20d-PO samples were prepared. Their pre-oxidation scale mean thickness was in the 8.7–17.8 μm range.

For the as-received alloys, Tables 3 and 5 also give the maximum sample temperature elevation, the time to transition and the ZrO_2 thickness at transition, whose meanings are discussed in the next section.

4. Results

4.1. As-received alloys

Fig. 4 gives on a log–log graph an overview of the TGA mass gain curves obtained with as-received Zircaloy-4 (Fig. 4(a)) and as-received M5® (Fig. 4(b)). The short duration tests dedicated to metallography are not plotted. For Zircaloy-4, at 1000, 1100 and 1200 °C,

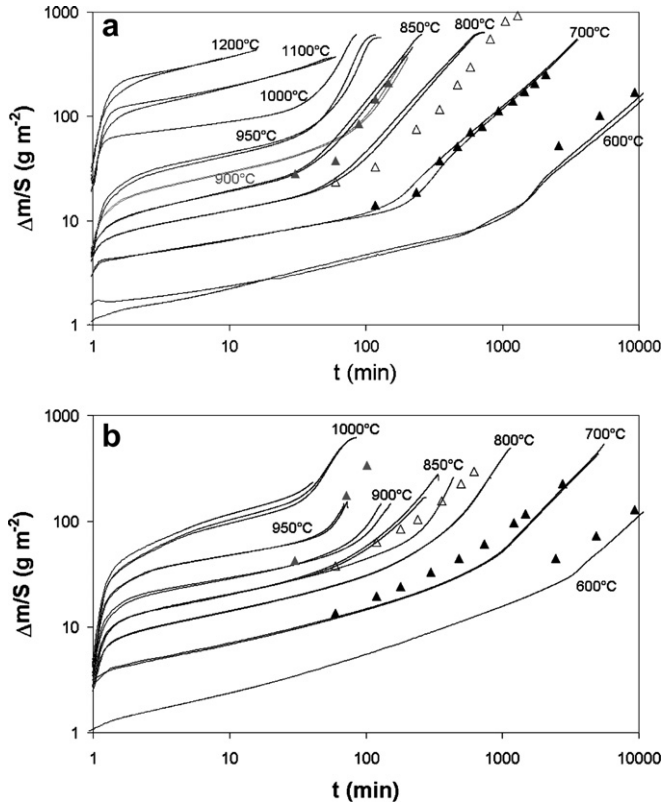

Fig. 4. Isothermal oxidation thermogravimetric results (mass gain per surface unit versus time) for the as-received bare alloys. Full lines: this study. Triangles: ANL results [3] at 600 and 700 °C (full black triangles), 800 (open triangles) and 900 °C (grey triangles). (a) Zircaloy-4 (b) M5®.

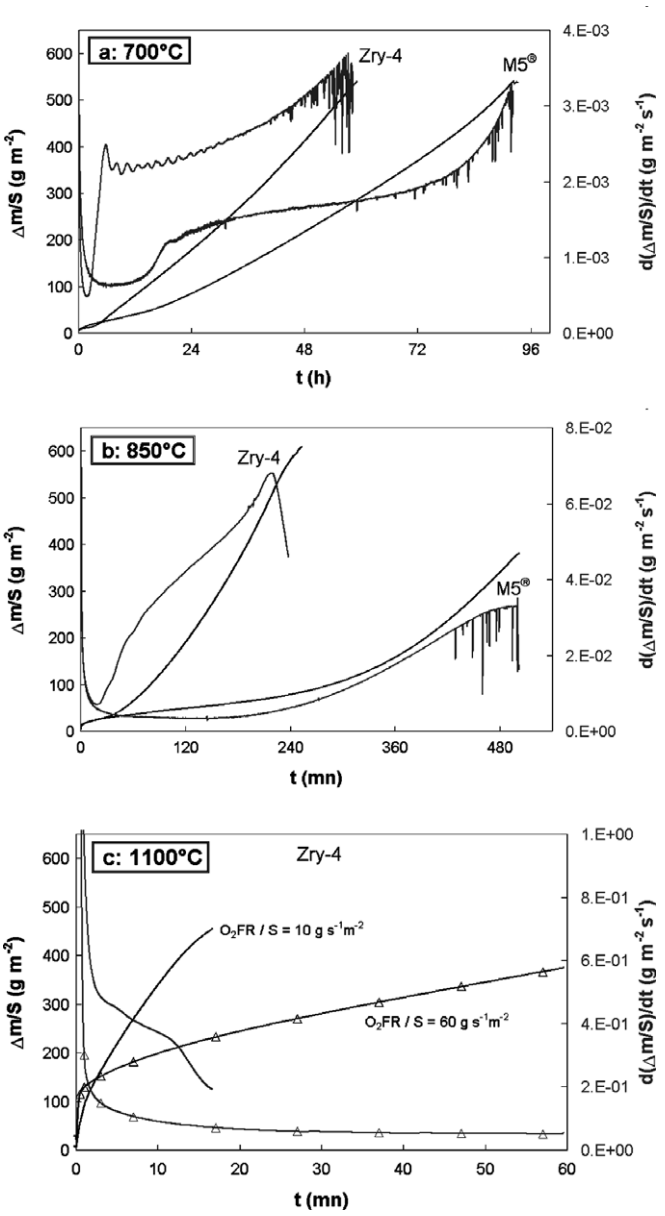

Fig. 5. Examples of isothermal air oxidation results on the bare 'as-received' Zircaloy-4 and M5® alloys. Black curves: Weight gain per surface unit (left *Y*-axis). Grey curves: oxidation rate calculated by derivation of the weight gain (right *Y*-axis). At 700 and 850 °C, comparison is done between Zircaloy-4 and M5®. At 1100 °C, two tests on Zircaloy-4 are plotted: one performed with a 20 mm long sample and a 500 mL/mn air flow rate (i.e. O_2 flow rate/S = 10 g s^{-1} m^{-2}), the other (triangles) with a 7 mm long sample and a 1000 mL/mn air flow rate (O_2 flow rate/S = 60 g s^{-1} m^{-2}).

only the tests performed with short samples and high air flow rate, not influenced by oxygen starvation, are plotted. The reproducibility appears generally very satisfactory. However this was not the case at 1000 °C where one of the two tests performed with high air flow rate and short samples shows an unusual strong oxidation peak at the air admission. This last test is discarded for further calculations. On Fig. 4, our data are compared to the recent ANL data obtained by off-line weighting of bare cladding exposed to air at 600, 700, 800 and 900 °C [3]. Note that for the ANL study, the experiments were single side oxidation tests performed with 75 mm long closed tubes. The agreement between the two studies is judged satisfactory taking into account the different protocols used.

Plots of the oxidation rate (calculated by derivation of mass gain) on a linear scale give better visualisation of the kinetics. Examples of such plots are given on Fig. 5 for 3 temperatures. The heating phase is not shown in the graphs and the *X*-axis origin corresponds to the air admission. The left *Y*-axis is for the weight gain per surface unit (black curve), the right *Y*-axis is for the oxidation rate (grey curves). For each temperature and each alloy, only one test is plotted for clarity, except at 1100 °C, where two Zircaloy-4 tests are plotted, one test for each configuration (1st configuration: 20 mm long samples, 500 mL/mn air flow rate, O_2 flow rate/ sample surface = 10 g s^{-1} m^{-2}; 2nd configuration: 7 mm long samples, 1000 mL/mn air flow rate, O_2 flow rate/ sample surface = 60 g s^{-1} m^{-2}). The kinetic curves obtained with the as-received bare alloys generally show the succession of the following events: first, at the air admission, the oxidation rate shows a sharp increase corresponding to the sudden oxidation of the non-protected bare metal. The oxidation rate then decreases progressively, because of the formation of a protective oxide layer. Then, having reached a minimum, a transition occurs, and the reaction accelerates. The process finally slows down when little metal remains available. The results are discussed in the following paragraphs distinguishing the pre-transition phase, the transition, then the post-transition phase.

4.1.1. The pre-transition phase

because of the high enthalpy of the Zr + O_2 reaction, the peak oxidation is associated with an elevation of the sample temperature (see 6th column of Tables 3 and 5th column of Table 5). Negligible at 600 and 700 °C, it becomes significant at 800 °C (ΔT = 20 °C), despite the small samples size and the rather high gas velocities in the furnace. It sometimes reaches 250 °C for the

highest furnace temperatures (1000, 1100 and 1200 °C). It's all the more important that the cumulated oxygen uptake during the peak becomes very significant at high temperature. It means that the experimental conditions cannot always be considered as truly isothermal. Despite this deviation from isothermal conditions, square root of time plots show that the mass gain can be considered to obey a parabolic behaviour on a large part of the pre-transition phase:

$$\Delta m/S = k\,t^{1/2}, \quad k \text{ is a constant and } t \text{ is the reaction time}, \qquad (1)$$

and that the reaction progresses by oxygen transport though a growing oxide layer. It is generally admitted that, as long as the growing layer remains protective, anionic solid-state diffusion is the limiting mechanism for zirconium alloys oxidation. This has been clearly demonstrated in the case of oxidation in high-pressure water and in oxygen at 360 °C by tracer experiments [12].

Derivation of Eq. (1) gives

$$1/(\mathrm{d}\Delta m/\mathrm{d}t) = 2/(S.k)\;t^{1/2} \qquad (2)$$

A plot of the inverse of oxidation rate versus square root of time gives better visualisation of the parabolic behaviour. For each tests, k calculations are performed by linear regression on the linear portion of the $1/(\mathrm{d}\Delta\mathrm{m}/\mathrm{dt})$ versus $t^{1/2}$ curve (Fig. 6). For the tests performed at 1000, 1100 and 1200 °C with a 500 mL/mn air flow rate and long samples, the $t^{1/2}$ plots exhibit a clear slope change during the decrease phase (Fig. 6(c)). It means that a single parabolic assumption is not anymore valid, indicating a more complex reaction path. This is supported by the metallographic post-test inspections of the samples, which are presented and discussed later. A k rate constant is nevertheless calculated from the second slope, considered to be less affected by the sample temperature elevation at the air admission. Results of the k calculations are plotted in an Arrhenius form on Fig. 7, distinguishing the values obtained with the 500 mL/mn tests from the ones corresponding to the 1000 mL/mn, short sample tests. Above 1000 °C, for the 500 mL/mn tests, the k values obviously stand apart over the other data, thus confirming the mechanism change. Because the physical significance of the parabolic assumption is here doubtful, these values will not be considered for further fit of our data. They are plotted in grey on Fig. 7.

Five experimental correlations are also plotted on Fig. 7 for comparison: (1) The well known Baker–Just correlation, based on Zircaloy-2 oxidation experiments in steam between 1273 and 2033 K [13], (2) The Cathcart–Pawell correlation, based on oxidation experiments in steam between 1273 and 1773 K [14], (3) The Leistikow–Schanz correlation, derived from steam oxidation experiments on Zircaloy-4 in the 973–1873 K temperature range [15] and recently recommended in [16] for high temperature oxidation of Zircaloy-4 in steam up to 1800 K, in the pre-breakaway regime; (2) The Hayes–Roberson correlation derived from air oxidation experiments on pure Zr in the 698–1173 K temperature range [17]; (3) The Leistikow–Berg correlation, derived from air oxidation data on Zircaloy-4 in a 973–1523 K temperature range [2]:

Baker—Just: for steam, 1273 K $< T <$ 2033 K

$$k\,(\mathrm{kg\ m^{-2}\ s^{-1/2}}) = 20.2\ \exp(-95100/RT) \qquad (3)$$

Cathcart—Pawell: for steam, 1273 K $< T <$ 2033 K

$$k\,(\mathrm{kg\ m^{-2}\ s^{-1/2}}) = 6.02\ \exp(-83600/RT) \qquad (4)$$

Leistikow—Schanz: for steam, 973 K $< T <$ 1873 K

$$k\,(\mathrm{kg\ m^{-2}\ s^{-1/2}}) = 7.24\ \exp(-87100/RT) \qquad (5)$$

Hayes—Roberson: for air, 698 K $< T <$ 1173 K

$$k\,(\mathrm{kg\ m^{-2}\ s^{-1/2}}) = 0.3391\ \exp(-57196/RT) \qquad (6)$$

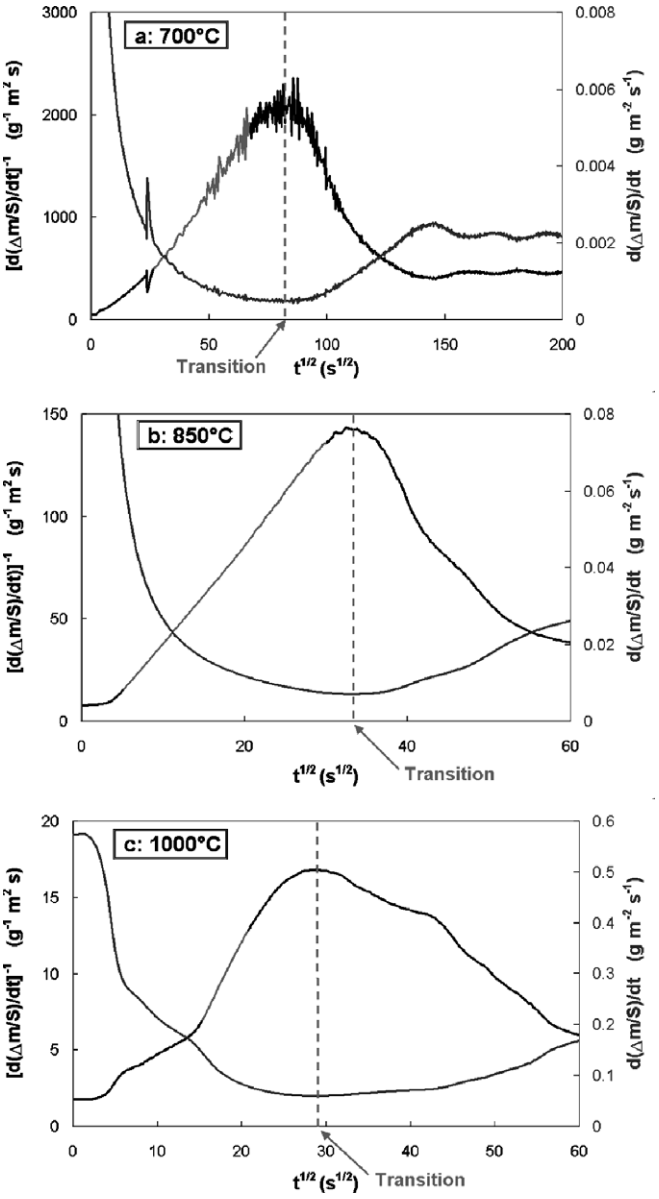

Fig. 6. Examples of $t^{1/2}$ plots for tests with 'as-received' Zircaloy-4. Black curves: Inverse of oxidation rate (left Y-axis). Grey curves: oxidation rate (right Y-axis). k parabolic rate constants are calculated by linear regression on the portion of the $1/(\mathrm{d}\Delta m/\mathrm{d}t)$ curves delimited in light grey.

Leistikow—Berg: for air, 973 K $< T <$ 1523 K

$$k\,(\mathrm{kg\ m^{-2}\ s^{-1/2}}) = 75.9\ \exp(-110860/RT) \qquad (7)$$

The two air correlations are used as the basis of two widely used recommendations for air ingress reactor severe accident analysis, generally referred as NUREG-1 and NUREG-2 [18]. These NUREG recommendations are conservative equations that take into account the high dispersion of the published air oxidation database. Our data are closer to the correlation for high temperature Zircaloy steam oxidation. It confirms that, in the solid-state-diffusion limited regime, oxidation kinetics are comparable in air and in steam, as already stated by Power et al. [18], and early suggested by Hayes and Roberson [17]. A fit of our data up to 1000 °C (1000 °C included, and not taking into account the values plotted in grey), gives

For Zircaloy-4, 873 K $< T <$ 1273 K

$$k\,(\mathrm{kg\ m^{-2}\ s^{-1/2}}) = 4.958\ \exp(-89403/RT(K)) \qquad (8)$$

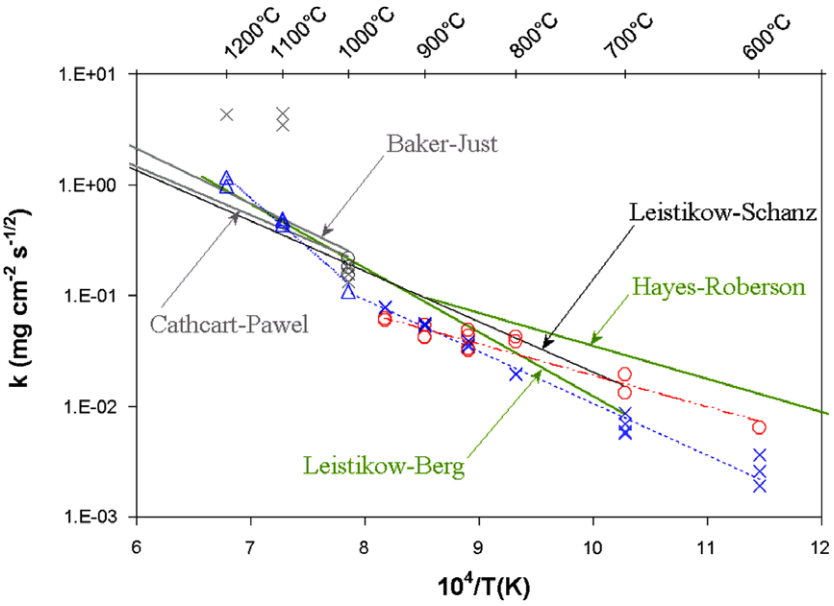

Fig. 7. Parabolic rate constants calculated from isothermal air oxidation tests. crosses: bare Zircaloy-4, 20 mm long samples, 500 mL/mn air flow rate. triangles: bare Zircaloy-4, 7 mm long samples, 1000 mL/mn air flow rate. circles: bare M5®, 20 mm long samples, 500 mL/mn air flow rate. Dotted lines are Arrhenius fits of the data. Data obtained at $T \geqslant 1000$ °C with 20 mm long samples, showing strong deviation from parabolic behaviour, are excluded from the fits and are plotted in grey. Hayes–Roberson correlation (Zircaloy-4 air oxidation, 698 K < T < 1173 K), Leistikow–Berg correlation (Zircaloy-4 air oxidation, 973 K < T < 1523 K), Leistikow–Schanz correlation (Zircaloy-4 steam oxidation, 973 K < T < 1800 K), and the well known Baker–Just and Cathcart–Pawel correlations (Zircaloy steam oxidation above 1273 K) are plotted as full lines for comparison.

showing activation energy very close to the one of the Leistikow–Schanz steam Eq. (5).

At 1000 °C, our data show a change in the activation energy and a fit in the 1000–1200 °C temperature range leads to

$$\begin{aligned} &\text{For Zircaloy-4, } 1273\ \text{K} < T < 1473\ \text{K} \\ &k\,(\text{kg m}^{-2}\ \text{s}^{-1/2}) = 1.50 \times 10^{4}\ \exp(-172305/RT) \end{aligned} \tag{9}$$

Tests performed with the bare M5® alloy also show at the air admission a fast oxidation peak followed by a parabolic decrease. The same "$t^{1/2}$ analysis method" has been applied to calculate parabolic k rate constants, also plotted on Fig. 7. For the lowest temperature, k rate constants for M5® are significantly higher than for Zircaloy-4, but k values merge above 800 °C. As was the case for Zircaloy-4, a slope change on the $1/(\mathrm{d}\Delta m/\mathrm{d}t)$ versus $t^{1/2}$ plots is observed for the tests done at 1000 °C and 500 mL/mn air flow rate, again indicating that the parabolic assumption is not anymore valid. Here, no tests were performed with shorter samples and higher air flow rate. Therefore, the 1000 °C data points are excluded for the fit that leads to the relation:

$$\begin{aligned} &\text{For M5®, } 873\ \text{K} < T < 1273\ \text{K} \\ &k\,(\text{kg m}^{-2}\ \text{s}^{-1/2}) = 0.1303\ \exp(-54250/RT) \end{aligned} \tag{10}$$

The activation energy of the diffusion process in the 873–1273 K temperature range thus appears to be significantly lower for M5 (Ea = 54.2 kJ/mol) compared to Zircaloy-4 (89.4 kJ/mol). This may be explained by differences in microstructure, crystalline structure and(or) stoichiometry of the dense zirconia layers grown on M5 and Zircaloy-4.

4.1.2. The transition

Thanks to the TGA on-line measurement technique, the minimum of the oxidation rate curves can be accurately located. The scale thickness for which the kinetic acceleration occurs is calculated from the weight gain at the minimum, assuming fully dense zirconia, and neglecting the contribution to the weight gain of the oxygen dissolved in the metal. On the other hand, post-test metallographic inspections reveal the presence of a dense zirconia surface scale, on both inner and outer side of the oxidised tubes (Fig. 8(a)–(h). For the highest temperatures, the columnar structure of this dense oxide is clearly visible. For each sample investigated, the mean thickness of this dense scale was determined by systematic measurements, including both the inner and the outer surfaces. The obtained values are plotted on Fig. 9 and are compared to the thickness at the kinetic transition calculated from the TGA curves, both for Zircaloy-4 and for M5®.

For Zircaloy-4, TGA and metallographic data are obviously strongly correlated. It clearly demonstrates that the dense oxide growths during the parabolic regime, and that the post-transition regime is associated with the growth of a 'porous' oxide, visible underneath the dense scale (here, the cracked structure is referred to 'porous', by opposition to the dense oxide). When the porous oxide is present, the dense scale shows penetrating radial cracks. The apparition of the porous oxide is thus closely associated with cracking of the dense zirconia. The observed kinetic transition can thus undoubtedly be referred to a 'breakaway transition'. In the next section, the post-transition formation of the 'porous' zirconia is proposed to be a consequence of the radial cracking of the dense oxide, which losses its protectiveness, rather than the reverse. Above 900 °C, the TGA data overestimate the dense oxide thickness, likely because at high temperature, oxygen dissolved in the metal contributes significantly to the mass gain. The fact that the dense surface scale thickness increases with temperature also means that an increasing part of the oxidation process occurs during the pre-transition parabolic regime. At 1100 °C and 1200 °C, for the tests at high air flow rate, where no kinetic transition is observed, only a very thick dense columnar oxide is seen on the metallographies.

On M5®, because of a higher dispersion, the correlation between the TGA data and the metallographic ones is less satisfactory (Fig. 9(b)). However, both the same type of zirconia structures, the dense columnar one and the cracked 'porous' one, are visible on the metallographies and are respectively attributed to the

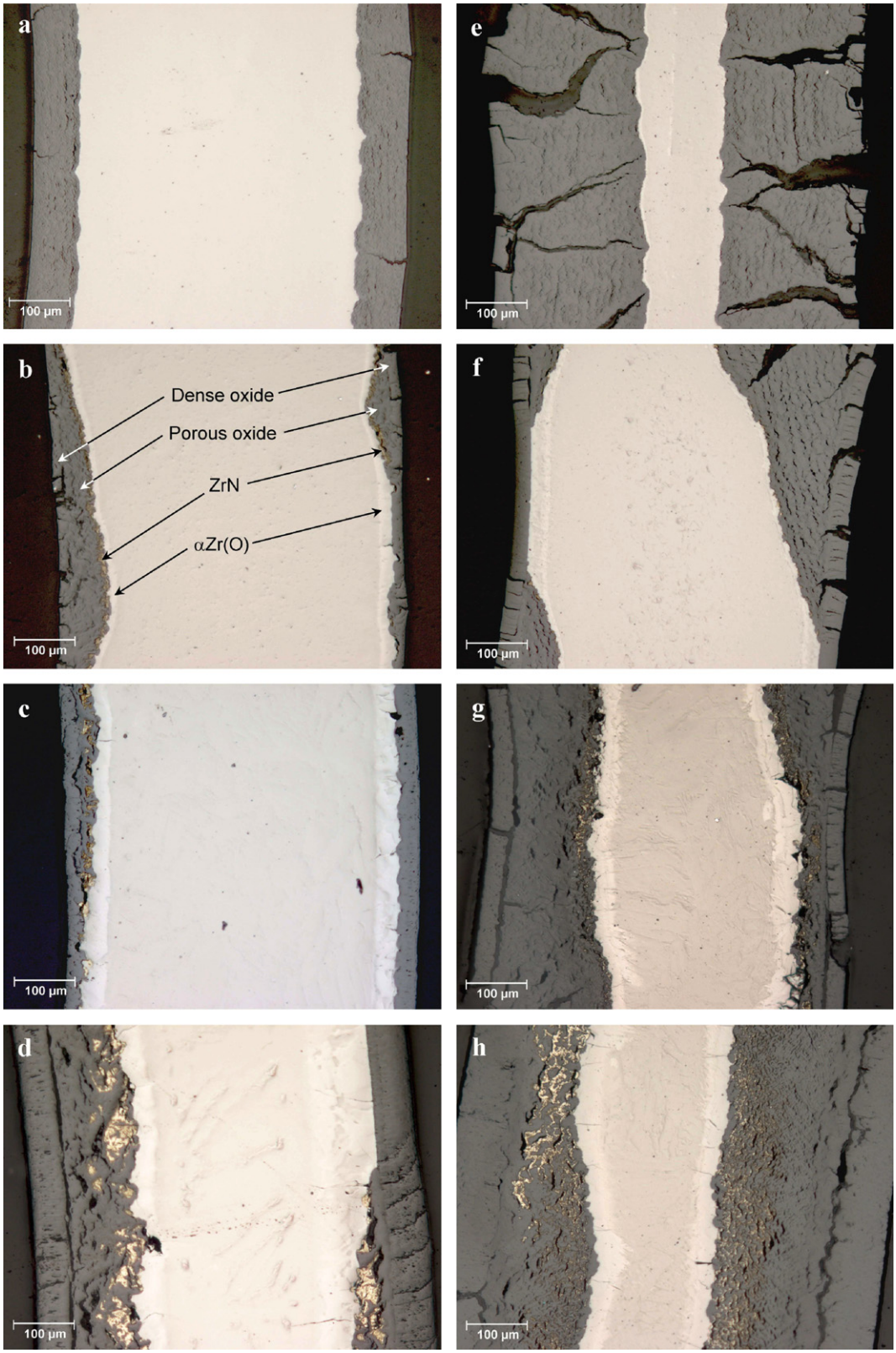

Fig. 8. Metallographies of initially bare samples after air oxidation. Conditions are given below (AED = air exposure duration, ECR = equivalent cladding reacted). (a) Zry-4, 700 °C, AED = 900 mn, 16.8%ECR (b) Zry-4, 850 °C, AED = 90 mn, 13.6%ECR (c) Zry-4, 950 °C, AED = 55 mn, 17.3%ECR (d) Zry-4, 1000 °C, AED = 103 mn, 76.1%ECR (e) M5®, 700 °C (f) M5®, 850 °C, AED = 340 mn, 42.8% ECR (g) M5®, 950 °C, AED = 110 mn, 61.1% ECR , AED = 5000 mn, 68.0% ECR (h) M5®, 1000 °C, AED = 40 mn, 37.3% ECR.

diffusion-limited parabolic growth and to the post-transition growth. At 600, 700 and 800 °C, compared to Zircaloy-4, the dense oxide that forms on M5® reaches a much higher thickness before cracking, and the radial cracks are thus very clearly seen. This is likely linked to the good corrosion behaviour of the M5® alloy at low temperature. It leads to a late transition, clearly visible on

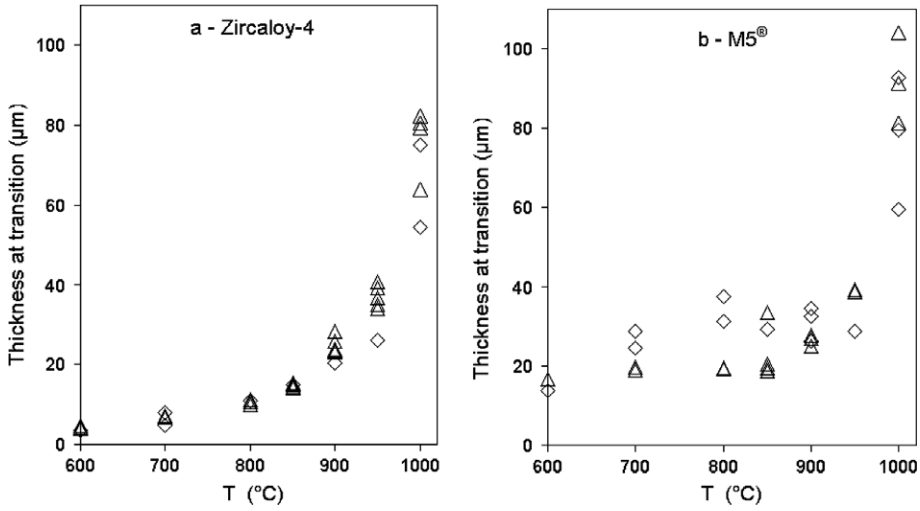

Fig. 9. Scale thickness at transition, calculated from the mass gain at minimum of the oxidation rate curve (triangles) and dense zirconia surface layer thickness, measured on the metallographies (diamonds), for as-received Zircaloy-4 and M5®.

the kinetic curves. Above 800 °C, the critical dense oxide thickness at which the breakaway occurs becomes similar for both alloys.

Such a significant temperature overshoot, even if transient, may have an impact on the oxide microstructure that forms during the pre-transition phase, and then on the time and thickness at transition. The putative consequences of temperature overshoots may be discussed by comparing, for a given final isothermal temperature, results obtained for different overshoot conditions. Unfortunately, our experimental database does not give such a possibility, because at a given temperature, the overshoot amplitude is rather constant from one test to another. At 1000 °C, however, some fluctuations are observed, but no obvious correlation between the overshoot amplitude and the thickness at transition is seen. One test shows an unexpectedly high oxidation rate peak and overshoot amplitude at the air admission (last test at 1000 °C in Table 3). The time at transition is somewhat shortened but the thickness at transition is not modified. For sure, no conclusion can be drawn on the basis of one test alone. The problem is still an open question. Understanding the dynamic growth and breakdown of a dense zirconia layer in transient non-isothermal conditions is undoubtedly very complex, and requires detailed microstructural investigations. Micro-Raman post-test studies of these oxide layers grown at high temperature are currently under consideration in our laboratory.

Another specific feature of this 800–1000 °C temperature domain is the strong axial and azimuthal heterogeneity of the breakaway: post-test inspections most often show bi-coloured samples, where areas still covered with the protective black hypostoichiometric zirconia coexist with brown or white regions, corresponding to areas where the breakaway has occured (Fig. 10(a) and (b)). Because of the better resistance of the M5® alloy to the breakdown of the protective oxide, this leads to situations where, on a 2 cm length, the metallic wall can be either nearly intact, or fully destroyed where the breakaway has early been initiated. Here, edge effects or scratches on the metal surface may have contributed to the breakaway initiation. The metallographies also clearly evidence the heterogeneity of the oxidation, and above 700 °C, micrographs selected to be presented on Fig. 8 are not indicative of the ECR, which is a global mean value given by the final mass gain. On micrographs 8b and 8f, it can clearly be seen that where the breakaway has occurred, the bright αZr(O) layer is much thinner than underneath the dense oxide, indicating a much faster progression of the oxidation front. The TGA technique gives a global measurement, but initiation of the breakaway, even if local, will

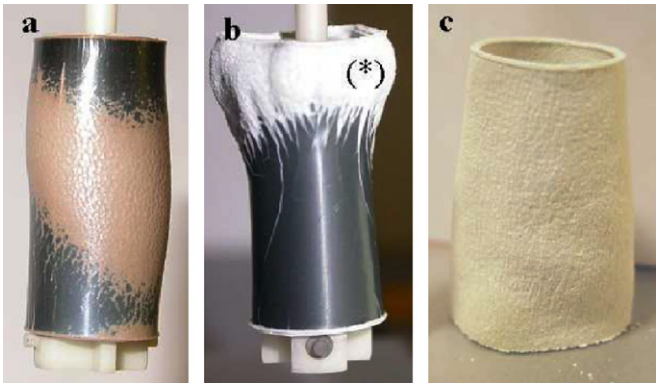

Fig. 10. Examples of samples oxidised in air at 850 °C. (a) 'as-received' bare Zry-4, air exposure 90 mn, ECR = 13.6%. (b) 'as-received' bare M5®, air exposure 260 mn, ECR = 26%. (c) pre-oxidised M5®, air exposure 160 mn, ECR = 55%. (*) The highly degraded white zone on M5® may be due to an end effect (early initiation of the breakaway on the edge).

undoubtedly induce a detectable increase of the mass gain rate. It means that any cause favouring such a local initiation of the breakaway, as scratches or end-effects, can induce an underestimation of the thickness at transition if calculated from the mass gained at the minimum of the rate curve. This may be the reason for the differences between TGA and metallographic data on Fig. 9(b), between 800 and 900 °C, for the M5 alloy, where end-effects are suspected. Anyway, it is of critical importance to point out that parabolic rate constant calculations are performed on portion of the rate curves before their minimum, that is for a time period where the breakaway has not been initiated anywhere. It means that the reaction is still diffusion controlled everywhere on the sample, and the calculation cannot be affected by the spatial inhomogeneity of the breakaway.

At 1100 and 1200 °C, temperature domain investigated only with the Zircaloy-4 alloy, TGA data do not show any transition to an accelerated regime and the oxidation rate continuously decreases in a parabolic way (Fig. 5(c)), provided that no oxygen starvation occurs. Samples appear homogeneously oxidised (Fig. 11(a)). On metallographies, a thick, unbroken dense zirconia layer is seen (Fig. 11(b)). Only big macroscopic cracks are observed (Fig. 11(a) and (c)).

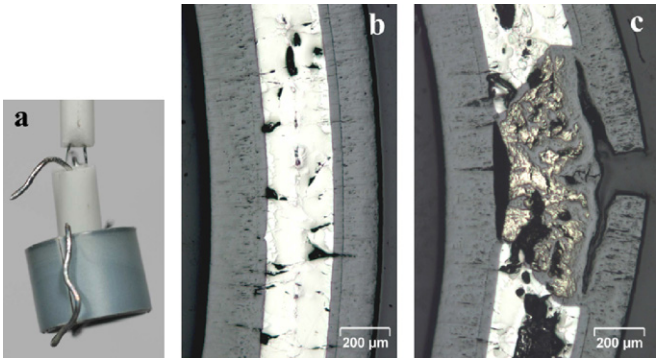

Fig. 11. 7 mm long Zircaloy-4 sample oxidised at 1100 °C in a 1000 mL/mn air flow rate (i.e. O_2 flow rate/S = 60 g s^{-1} m^{-2}), during 60 mn, ECR = 58.6%. (a) Macrophotography. (b) Metallography. (c) Metallography at the axial crack location.

4.1.3. The post-transition phase

At 600 °C and 700 °C, the transition to high oxidation rates is abrupt, both for Zircaloy-4 and for M5®. The post-transition oxidation rate rapidly stabilises (linear regime) showing only further moderate increase. For Zircaloy-4, small oscillations can be seen to superimpose to the linear kinetics (Fig. 5(a)). A stratified oxide is very clearly seen on the post-tests metallographies (see Fig. 8(a)). The layer thickness is in the 10–15 μm range, in coherence with the mass gained between the oscillations of the oxidation rate. As already mentioned, the same kind of periodic feature is often reported for corrosion scales grown on Zircaloy-4 upon 'in-use' PWR conditions, and has also been correlated to kinetic periodic oscillations using in situ impedance spectroscopy [5]. For M5®, the post-transition rate is significantly lower than for Zircaloy-4. The stratification of the post-transition oxide is also visible (Fig. 8(e)), however we do not observe oscillations on the thermogravimetric curves.

At 800 °C and above, rather than an abrupt transition and a constant post-transition rate, the oxidation rate shows a progressive and continuous increase after the minimum, up to very high ECR. Here, it has to be recalled that TGA is a global measurement, and that the mass gain measured in the post-transition phase is a spatial average of values that can be strongly different from one place to another. Thus, progressive propagation of the locally initiated breakaway can be a major cause of the progressive acceleration observed after the transition. At 800 and 850 °C, the M5® alloy shows a moderate post-transition acceleration compared to Zircaloy-4, however this hides the fact that the degradation rate can be locally very high. In the 900–1000 °C temperature range, the post-transition kinetics are not anymore significantly different for the two alloys. On the metallographies, the stratification of the oxide evidenced at low temperature disappears progressively, to give place to a more disorganised structure. On Zircaloy-4, the stratification has fully disappeared from 850 °C, while on M5® it is visible up to 900 °C. The stratification clearly appears to be parallel to the metal/oxide interface (and not to the external surface). It is a strong indication that the fissuring occurs by periodic buckling and detachment from the metal of the last-formed oxide layer, as it is probably the case for the corrosion scales (see Section 2). Correlatively, yellow particles, known to be the ZrN compound [1], are seen embedded in the oxide, nearby the metal/oxide interface. When increasing the oxidation temperature, their size, density and extend into the oxide increase as the stratification disappears. For a given temperature, more nitride is seen for Zircaloy-4 than for M5®. Hardly seen as scarce and tiny precipitates in contact with the metal for M5® oxidised at 800 °C, the nitride forms big islands dispersed into a several tenth of micron deep oxide zone at 1000 °C.

It is also worth pointing out that there is strong sample deformation where the porous oxide has grown, for both alloys. It has been shown that even at moderate temperature, tensile stress applied on the metal by a corrosion layer can induce detectable creep-growth [19]. For the temperatures investigated here, much higher creep can be expected. When no nitride formation is seen (600 and 700 °C), the oxidation process is spatially uniform and the samples keep their cylindrical shape. Growth can be quantitatively estimated by sample size measurements: On Zircaloy-4, we have measured at 600 °C values of $\Delta L/L$ of 1.5% (at 14% ECR) to about 5% (at 45% ECR). From 800 °C, growth is moderate where the surface is covered with the black oxide, but huge growth is seen where the transition has occurred, leading to ballooning or even to tulip or cauliflower shapes. Such strong deformations of the cladding obviously induce very significant increase of the exposed metal surface during the oxidation tests.

4.2. Pre-oxidised samples

4.2.1. Zircaloy-4

With the moderately pre-oxidised samples (20d-PO), the initial oxidation rate peak is strongly attenuated and the time to reach the transition is shortened (Fig. 12(a) and (b)). For the lowest temperatures investigated (600 and 700 °C), the duration of the pre-transition regime is even negligible. The mass gained before the transition becomes noticeable above 800 °C. However, on the metallographies, no dense oxide layer is seen underneath the pre-oxidation scale (except at 1000 °C). The post-transition kinetics are not much modified by this moderate pre-oxidation (Fig. 12(a) and (b)).

With 60d-PO samples, this is not the case, TGA data showing significantly lower post-transition rates in the 700–850 °C range (Fig. 12(a)). A 60–80 μm thick 'corrosion' layer (high burn-up simulation) thus clearly has a limiting effect up to 850 °C, slowing down the degradation upon air exposure. For higher temperatures, this limiting effect is not anymore noticeable (Fig. 12(b)). The degradation kinetics become even faster at 1100 °C with the 60d-PO samples, compared to the as-received alloy (Fig. 12(c)). When with the bare alloy only a parabolic decreasing regime was seen, with the pre-oxidised samples, in the same test conditions, the degradation rate accelerate after an 'incubation' time.

On the metallographies, in the 600–1000 °C temperature range, both for 20d-PO and 60d-PO samples, the oxide that has grown under the corrosion layer is very similar to the post-transition oxide grown on the as-received alloy: stratified at low temperature (Fig. 13(a)), more disorganised and associated with nitride particles at the metal–oxide interface above 800 °C (Fig. 13(b)). At 1100 °C, temperature investigated only with the 60d-PO samples, a porous oxide with a high density of nitride is seen under the corrosion oxide (Fig. 13(c)), when in the same conditions, only a dense oxide scale was observed with the as-received cladding (Fig. 11(b)). It is clear here that the corrosion layer promotes ZrN formation. At 1200 °C, the 'corrosion' oxide looses its mechanical integrity (likely because of the monoclinic to tetragonal phase transformation of the zirconia grown at 500 °C when heated at 1200 °C) and therefore has no more effect, neither protective nor detrimental. The kinetics are unchanged compared to the as-received alloy, and the oxide grown under the corrosion layer is quite similar to the one grown on the bare alloy, even if somewhat less regular (Fig. 13(d)). Nitride are only barely seen.

4.2.2. M5®

Only moderate thickness 'corrosion' layers were prepared on M5®. As for Zircaloy-4, the first noticeable effect is a strong attenuation of the oxidation rate peak at the air admission. The time to transition also decreases with pre-oxidised M5. This is not so

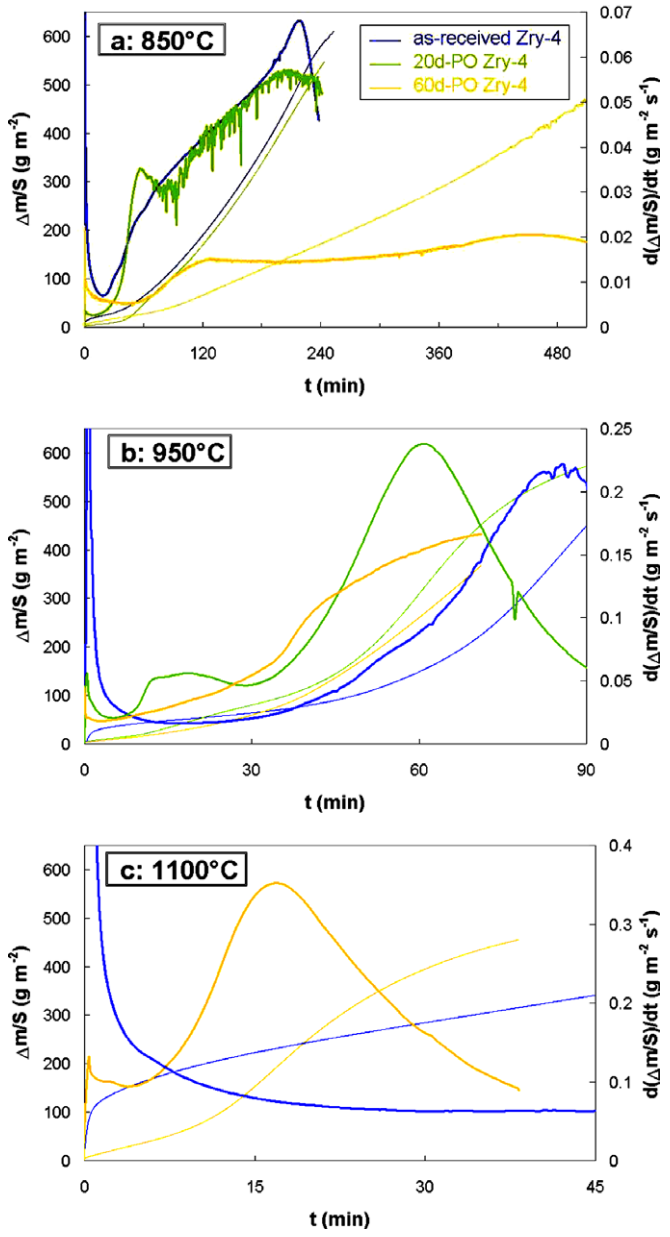

Fig. 12. Comparison of isothermal oxidation TGA results, at 850, 950 and 1100 °C, for 'as-received', 20 days pre-oxidised or 60 days pre-oxidised Zircaloy-4. Mass gain curves (left *Y*-axis) are plotted as fine lines, oxidation rate curves (right *Y*-axis) are plotted in bold.

significant at 700 °C, where the TGA curves for as-received and pre-oxidised M5 merge (Fig. 14(a)). At 800 °C, the time to transition is significantly shorten, and the difference becomes huge at 850 °C (Fig. 14(b)), 900 and 950 °C. On the metallographies however, a dense oxide is always visible underneath the pre-oxidation layer. Regarding the post transition regime, there is no or very little effect of the pre-oxidation at 700 and 800 °C, respectively, but from 850 °C, the pre-oxidation induces strong acceleration of the degradation (Fig. 14(b)). At 900 and 950 °C, reaction runaway and large temperature escalation were systematically observed with the pre-oxidised samples, after ~50 mn air exposure at 900 °C (Fig. 14(c)) and ~20 mn air exposure at 950 °C. Post-test inspections show that the transition is spatially more uniform for these pre-oxidised samples than for the bare ones (see Fig. 10(c)). At 1000 °C, runaway is not anymore observed and the TGA curves obtained with the pre-oxidised samples merge with those of the 'as-received' ones.

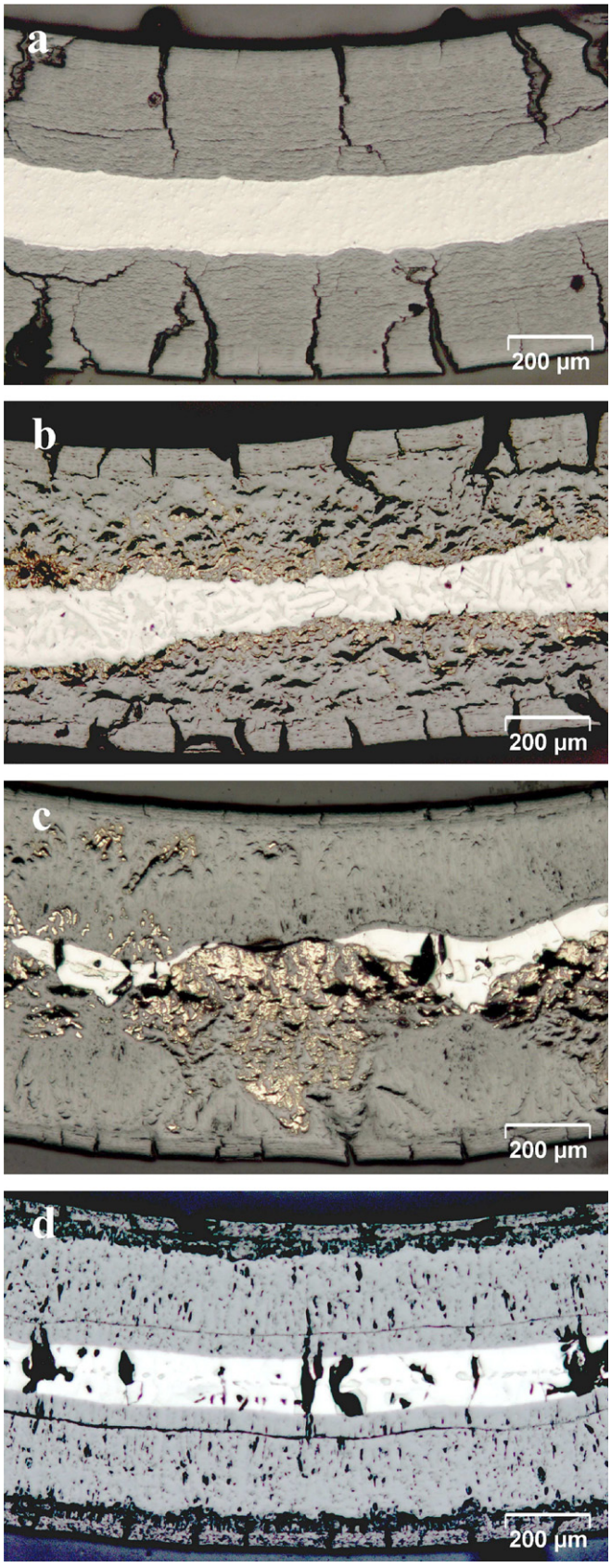

Fig. 13. Metallographies of Zircaloy-4 samples initially pre-oxidised in steam at 500 °C during 60 days, then oxidised in air at conditions given below (AED = air exposure duration, total ECR = ECR in steam + ECR in air). (a) 700 °C, AED = 85.3 h, total ECR = 66.2%. (b) 1000 °C, AED = 73 min, total ECR = 87.6%. (c) 1100 °C, AED = 27 min, total ECR = 83.9%. (d) 1200 °C, AED = 33 min, total ECR = 86%.

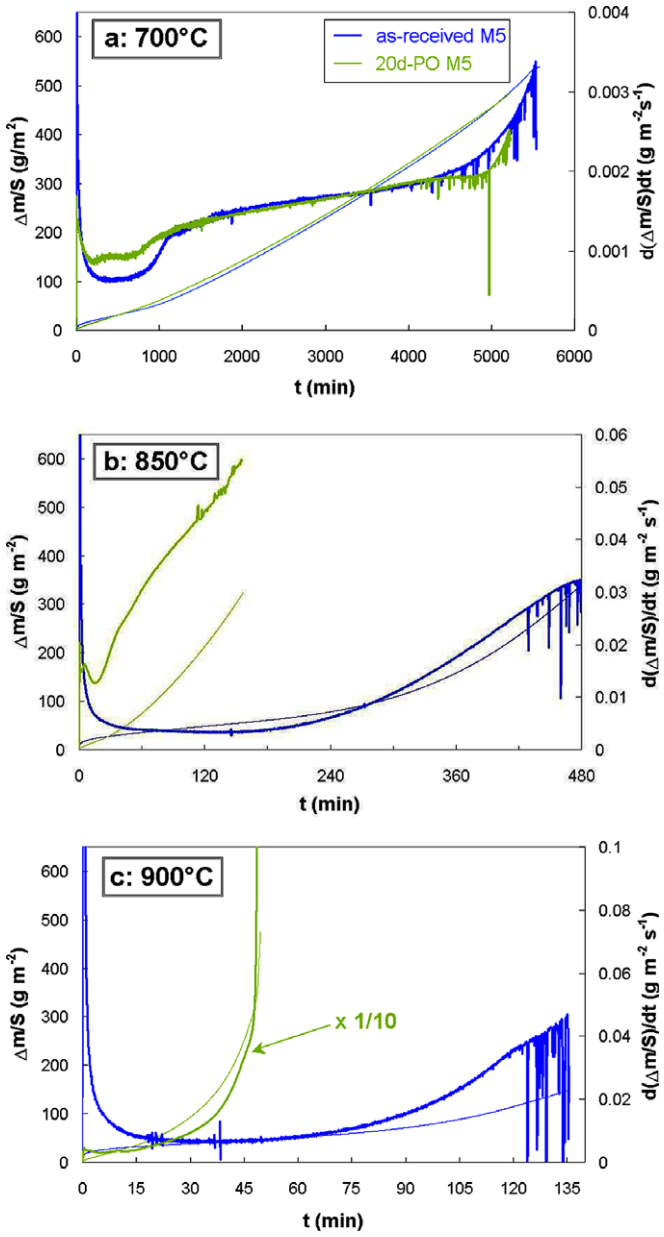

Fig. 14. Comparison of isothermal oxidation TGA results, at 700, 850 and 900 °C, for 'as-received' and 20 days pre-oxidised (20d-PO) M5®. Mass gain curves (left *Y*-axis) are plotted as fine lines, oxidation rate curves (right *Y*-axis) are plotted in bold.

4.3. Effect of gas phase oxygen starvation

At 1100 °C and 1200 °C, for tests done on the bare metal with 7 mm long samples, with a 1000 mL/mn air flow rate and with the 'opened' sample holder, the maximum oxygen consumption, calculated from the TGA data, does not exceed during the peak 20–35% of the oxygen injected (at 1100 °C and 1200 °C, respectively). The samples are uniformly covered with a dense oxide scale (Fig. 11(b)). Nitriding is not observed, except locally, where macroscopic cracks have formed along the axial direction (Fig. 11(c)).

Conversely, for tests done with 20 mm long samples and a 500 mL/mn air flow rate, the oxygen consumed/oxygen injected ratio reaches very high instantaneous values (70–95%), just after the air admission. Moreover, the oxidation rate at peak maximum is significantly lower than for the previous high flow rate tests. Thus, transient oxygen starvation can be suspected, especially for

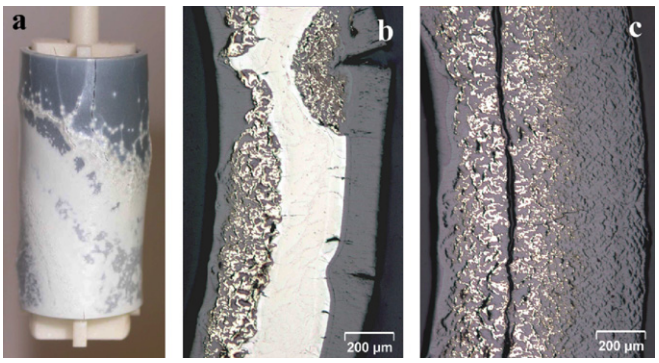

Fig. 15. 20 mm long Zircaloy-4 sample oxidised at 1100 °C in a 500 mL/mn air flow rate (i.e. O_2 air flow rate/S = 10 g s^{-1} m^{-2}), during 14 min, ECR = 70.4%. (a) Macrophotography. (b) Metallographic cut, upper part (local starvation at the bottom of the big crack or inside the tube). (c) Metallographic cut, lower part (local starvation inside and outside the tube).

downstream sample zones. Actually, post-test inspections reveal strong differences between the upper part and the lower part of the samples: a thick dense black oxide scale covers the upper part of the outside surface, whereas a white porous oxide, associated with extended nitriding, and whose structure is similar to the one of the post-breakaway oxide of the lower temperature tests, has formed downstream (Fig. 15). It is worth noticing that here, the porous structure often grows from the beginning of the metal attack, that is with no dense oxide top layer. On the inside surface, where the air access can be limited by the sample holder, nitriding is also very intense.

It is clear from these observations that oxygen starvation in the gas phase can initiate nitride formation even for temperature where no nitride forms if no starvation occurs. It results in a faster cladding degradation, as shown by the TGA data presented in Fig. 5(c). Such enhanced cladding degradation associated with porous oxide formation and extended nitriding has already been reported: In the QUENCH-10 bundle experiment conducted at FZK, it was proposed that the strong degradation of the bundle was the result of nitride formation (from the pre-existing oxide, because of extended oxygen starvation during the air-ingress phase), and re-oxidation during the final quenching phase [20]. The mechanism of this fast, nitrogen-associated degradation is discussed in the next section.

5. Discussion

On the bare metal, for Zircaloy-4 as well as for M5®, air oxidation at high temperature first gives rise to the growth of a dense protective oxide. The kinetic regime is a solid-state diffusion limited regime and the TGA data are satisfactorily fitted by a parabolic law. For Zircaloy-4, an Arrhenius plot of the calculated parabolic rate constants gives apparent activation energy very close to the value recommended in a recent assessment of the literature data for Zircaloy-4 steam oxidation at high temperature [16]. This suggests similar properties of the oxides grown in air and in steam regarding oxygen diffusion. For M5®, the rate constants are significantly higher than for Zircaloy-4 in the lower part of the temperature range investigated (under 850 °C). Literature data on M5® oxidation at high temperature are scarce, and mainly concern the 1000–1200 °C temperature range, relevant of LOCA conditions. Portier et al. have compared oxidation kinetics for low tin Zircaloy-4 and M5® in steam at 1000, 1100 and 1200 °C [21]. At 1000 °C, the reaction rate in the pre-breakaway regime is shown to be significantly lower for M5® than for Zircaloy-4. As discussed in Section 4.1 our reaction rate coefficient calculated at 1000 °C for

M5® have to be discarded, because oxygen starvation is suspected. However, extrapolation of our 600–950 °C data at 1000 °C leads to a k value of 0.077 mg cm^{-2} s$^{-1/2}$, in rather good agreement with the 0.11 mg cm^{-2} s$^{-1/2}$ k value calculated from the 1000 °C M5 mass gain data of Ref. [21].

Above 1000 °C, Zircaloy-4 exhibits an higher activation energy (temperature domain not investigated for M5® in this study). Changes of the activation energy of the diffusion limited regime have been early reported for Zircaloy steam oxidation, at about 900 °C and 1600 °C, and kinetic correlations distinguishing the 3 allotropic domains of the zirconia have were proposed [22]. Our data can also probably be related to the zirconia tetragonal-monoclinic transformation, which is given to occurs for pure zirconia between 950 °C and 1050 °C [23]. Because the breakdown of zirconium alloys oxidation scales is known to be associated with this ZrO_2 allotropic transformation [24], the absence of breakaway for the tests at 1100 and 1200 °C is another strong indication that a microstructural change of the dense scale occurs above 1000 °C. In steam, absence of breakaway when temperature exceeds 1000 or 1050 °C has been reported by several authors, for Zircaloy-4 [25,21,26], as well as for M5® [21] and for a Zr–1Nb–1Sn–0.1Fe alloy [26].

Breakdown induces loss of the scale protective effect. For temperature above 800 °C, where nitriding is observed under the broken dense zirconia scale for both alloys, the following sequence of events, leading to the formation of a porous oxide and an acceleration of the degradation, is proposed: to relieve high compressive stresses accumulated in the oxide, cracks form in the radial direction, when the oxide reaches a critical thickness, along the columnar grain boundaries, giving direct access for the air to the metal. Here, oxygen is consumed rapidly, which creates, at the bottom of the cracks, local oxygen starved situations. A pure nitrogen atmosphere remains, which is then able to react either with the α-Zr(O) phase or the sub-stoichiometric oxide [27], both available at that place, to form the ZrN compound in a spotwise manner. As the oxidation front further progresses inward, the nitride islands become embedded in the oxide, where they are re-oxidised by newly available oxygen flowing from the external surface to the metal. Due to the high volume increase associated with the ZrN–ZrO_2 conversion (ZrN molar volume = 14.8 cm^3, ZrO_2 molar volume = 21.7 cm^3, leading to a $\Delta V/V$ ratio of 46%), the oxide scale is submitted to local high stresses and breaks. The spotwise nature of this nitriding–oxidation process can then explain the disorganised cracks arrangement of the oxide grown under its influence, compared to the layered cracks network observed at lower temperature and generated as the effect of a more uniform compressive stresses field.

Optical dark field microscopic images give more information on the high temperature oxidation process, as illustrated by Fig. 16. One can clearly distinguish four regions in the oxide layers:

- The most external one (labelled region 1 on Fig. 16) is the dense columnar oxide grown during the parabolic regime. Where the breakaway has occurred, it is interspersed with micro-cracks, visualised by the dark-field illumination. It means that the coarse radial cracking visible on the bright field image is associated with micro-cracking, likely induced by the phase transformation of the initially tetragonal grains into the monoclinic structure, when the compressive stresses are relaxed [24]. This micro-fissuring undoubtedly contributes to the loss of protectiveness of the scale.Underneath, the porous oxide formed under the influence of nitrogen is composed of 3 sub-layers:
- The most internal one (region 4), in contact with the metal, contains nitride particles. When in contact with ZrN [28] or when exposed to a nitrogen atmosphere [29], zirconia dissolves nitrogen in its anion sub-lattice. Nitrogen is thus likely present in solution in the zirconia of region 4 and stabilises the tetragonal phase [30].

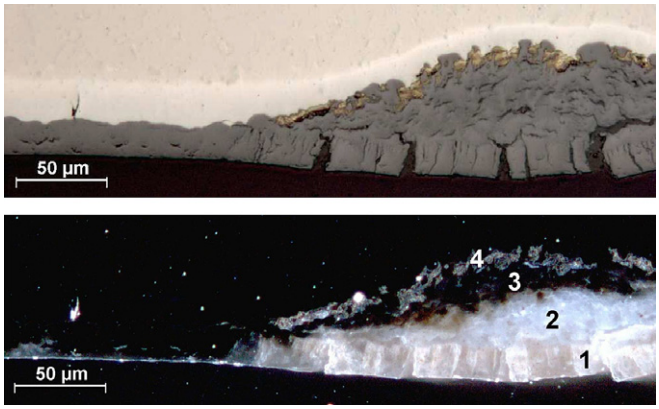

Fig. 16. Bright field and dark field optical metallographies of as-received Zircaloy-4 oxidised in air at 850 °C.

- Just above (region 3), ZrN has converted into oxide, leaving a cracked oxide.
- Region 2 has the same appearance than region 3 in the bright field image, but is illuminated in the dark field mode, while it is not the case for the region 3 layer. It means that micro cracking has occurred: Nitrogen, still dissolved in the zirconia of region 3, was progressively replaced by oxygen, inducing the tetragonal to monoclinic phase conversion. The region 2 oxide is thus not only 'macro-cracked', but also 'micro-porous', as it is the case in region 1.

Only detailed crystallographic investigations might confirm the exact nature of this nitrogen-associated phenomenology. Anyway, once initiated, the nitride-assisted degradation will be a self-sustaining process, because ZrN conversion into oxide leaves nitrogen trapped in the oxide scale and available for further nitriding, and because the oxide formed is undoubtedly non-protective. Where nitriding has initiated, the bright α-Zr(O) layer is thin, confirming the faster progression of the oxidation front there. The self-sustainability of the nitriding-reoxidation sequence may also favour the lateral progressive propagation of the breakaway.

At 1100 °C and 1200 °C, even though no global breakdown of the dense oxide occurs, intense nitriding is systematically observed where big, axially oriented fissures have formed (Fig. 11(c)), inducing local destruction of the cladding wall. The same nitriding-reoxidation sequence, initiated by a local oxygen starved situation inside the big fissure, can explain this local strong degradation. More extended oxygen starvation was encountered for the tests performed at 1100 and 1200 °C with insufficient air flow rate injected. Here, the nitride-associated, defective oxide widely spread on the samples surface and lead to durable, fast mass gain rate, even if the starvation was only a short transient situation. This clearly confirms the self-sustainability of the nitride-assisted oxidation once initiated.

At that point, we understand that any situation generating oxygen-starved conditions in the gas phase will favour initiation of the nitride-associated fast degradation. A cracked 'corrosion' scale is not protective, but is a porous media that limits the gas phase mass transport to the metal. As it was proposed for a radially cracked dense oxide scale, we thus suggest that oxygen starvation can occur in the porosities of a 'corrosion' scale, close to the metal/oxide interface, after consumption of the limited amount of oxygen available. It follows nitriding initiation and an early transition to the accelerated kinetic regime, as indeed observed with our pre-oxidised samples, both for Zircaloy-4 and for M5®. When the corrosion scale is thick (high burn-up spent fuel), the gas phase mass transport limitation would be high enough to prevent a too strong

acceleration of the reaction. It could explain the moderate post-transition degradation rate observed in the 700-850 °C temperature range for the 60d-PO Zircaloy-4 samples. Thus, the effect of the corrosion scale is here beneficial. However, it has to be pointed out here that the pre-oxidation conditions used in this study induce strong hydrogen loading in the metal. The high hydrogen content of our samples may have somewhat influenced the TGA results. Experiments with more representative corroded claddings would be desirable.

A key point to be discussed is the continuous increase of the mass gain rate we have measured above 800 °C in the post-breakaway regime, when linear kinetics is usually expected. Evans has early suggested that strong sample deformation generally observed in air oxidation experiments can be a consequence of the nitriding-oxidation sequence [1]. Indeed, in our experiments, sample deformation is strong only where nitriding have occurred. Such deformation is likely due to creep of the metal upon the stresses applied by the oxidation scale when nitride particles convert into oxide. It induces a very significant increase of the surface exposed to air, which undoubtedly contributes to the post-breakaway acceleration. Actually, we have recently performed few oxidation tests (not reported here) with hydrogen loaded (~600 ppm) Zircaloy-4 cladding. The breakaway initiation appears to be spatially very uniform with these samples, probably because the electrolytic process used for hydrogen loading induces a degradation of the surface state of the cladding. The thermogravimetric curves then show a more abrupt transition, but the post-transition kinetics remains continuously accelerated. Because of the high spatial uniformity of the oxidation with these hydrogen-loaded samples, it was possible to measure the sample size after the tests. Tests were stopped after variable exposure duration (i.e. for different final ECR), and the slope of the oxidation rate after the transition has been quantitatively correlated to the sample surface increase measured after the tests. Therefore, it is demonstrated that the strong creep of the cladding metallic wall associated with nitriding is a major contribution to acceleration of the degradation after the transition. For as-received samples, the continuous acceleration the degradation rate observed after the kinetic transition is a combined effect of this creeping process and of the progressive propagation of the breakaway over the sample surface.

6. Conclusions

For nuclear facility safety analysis purposes, the Zircaloy-4 and M5® air oxidation at high temperature has been investigated by thermogravimetry, first with as received bare cladding tubes, then with samples pre-oxidised at low temperature (500 °C) in steam to simulate in-reactor corrosion. On the bare alloys a protective dense zirconia scale first grows, giving rise to a solid-state diffusion limited regime, which can be described by parabolic kinetics. Comparison with literature data shows that existing parabolic recommendations for air oxidation are strongly conservative and that our data better fit with recently recommended steam correlations.

However, parabolic kinetics can only describe a limited time window of the cladding degradation. Breakdown and loss of the dense scale protective effect occur and result in an accelerated degradation. The scale thickness at breakaway has been determined in isothermal conditions as a function of the temperature. In the as received bare state, up to 850 °C, M5® appears much more breakaway-resistant than Zircaloy-4, and forms much thicker protective scales. But for pre-oxidised claddings, this advantage is lost, because the nitriding is favoured by the 'corrosion' scale: The transition occurs earlier than with the bare cladding, for both alloys. A reasonable conservative approach for safety analysis can then be to only consider post-breakaway kinetics.

Till 700 °C, the acceleration at breakaway is moderate and the oxidation rate stabilises to a linear regime. At 800 °C and above, continuous acceleration is observed, as the consequence of a complex process involving nitride formation and re-oxidation, as well as dissolution of nitrogen in the zirconia anion sub-lattice. Important volume mismatches of the ZrO_2 and ZrN compounds, together with zirconia phase transformations lead to growth of a highly cracked, porous, non-protective oxide. It results in fast progression of the oxidation front, as well as strong deformation of the cladding. The barrier against fission product release provided by the fuel cladding is lost much earlier than during accident under steam atmosphere.

Kinetic data of this study have been obtained mainly in high air flow conditions. In real accidental situations, where oxygen starved situations are likely to occur, cladding degradation can be even much faster than predictable from these high air flow data, because of early initiation of the nitriding process, as shown by the few tests performed at the highest temperatures with insufficient air flow rate. All in all, more experimental investigations are required to address the various conditions that can be encountered in accidental situation. For that perspective, tests involving exposures to N_2 rich atmospheres or air + steam atmospheres are foreseen. Situations with sequential exposure to N_2 then to air have also to be considered. Last but not least, tests addressing temperature transient conditions are also undoubtedly essential.

In other respects, thorough microstructural investigations of oxidation scales are under consideration to bring a more detailed mechanistic understanding of the nitrogen-associated fast degradation process.

Acknowledgements

Dr Martin Steinbrück from FZK is thanked for discussions having contributed to propose the nitrogen assisted degradation phenomenology. Many thanks to Dr Olivia Coindreau for her careful rereading of the manuscript.

This program was conducted within the framework of the International Source Term Program, funded by IRSN, Commissariat à l'Energie Atomique, Electricité de France, the European Commission, the US-Nuclear Regulatory Commission, the Paul Sherrer Institut, and Suez/Tractebel.

References

[1] E.B. Evans et al., Critical role of nitrogen during high temperature scaling of zirconium, in: Proceedings of the Metallurgical Society of AIME Symposium on High Temperature Gas–Metal Reactions in Mixed Environments, Boston, 9–10 May 1972.
[2] S. Leistikow, H.V. Berg, Investigation under nuclear safety aspects of Zircaloy-4 oxidation kinetics at high temperatures in air, in: Proceeding of the 2nd Workshop of German and Polish Research on High Temperature Corrosion of Metals, Julich, 2–4 December 1987.
[3] K. Natesan, W.K. Soppet, Air Oxidation Kinetics for Zr-based Alloys, Argonne National Laboratory Report 03/32, NUREG/CR-6846, Nov. 2003.
[4] A. Yilmazbayhan, E. Breval, A. Motta, R. Comstock, J. Nucl. Mater. 349 (3) (2006) 265.
[5] J. Schefold, D. Lincot, A. Ambard, O. Kerrec, J. Electrochem. Soc. 150 (10) (2003) B451.
[6] P. Bossis, D. Pêcheur, K. Hanifi, J. Thomazet, M. Blat, Comparison of the high burn-up corrosion on M5 and low tin Zircaloy-4, Zirconium in the Nuclear Industry, in: Fourteenth International Symposium, ASTM special technical publication 1467, 2004, p. 494.
[7] J. Godlewski, J.P. Gros, M. Lambertin, J.F. Wadier and H. Weidinger, Raman Spectroscopy Study of the Tetragonal-to-Monoclinic Transition in Zirconium Oxide Scales and Determination of Overall Oxygen Diffusion by Nuclear Microanalysis of O18, Zirconium in the Nuclear Industry, 9th International Symposium, ASTM special technical publication 1132, 1991, p. 416.
[8] A.M. Huntz, M. Andrieux, R. Molins, Mater. Sci. Eng. A 417 (1-2) (2006) 8.

[9] H.E. Evans, A. Stawbridge, R.A. Carolan, C.B. Ponton, Mater. Sci. Eng. A 225 (1997) 1.
[10] M. Blat, D. Denoel, Detrimental role of hydrogen on the corrosion rate of zirconium alloys, Zirconium in the nuclear industry, Garmish-Partenkirschen, 1995, ASTM Special Technical Publication 1295, 1996, p. 319.
[11] K. Natesan, W.K. Soppet, Hydrogen effects on air oxidation of Zirlo alloy, Argonne National Laboratory Report 04/14, NUREG/CR-6851, Oct. 2004.
[12] A. Grandjean, Y. Serruys, J. Nucl. Mater. 273 (1999) 111.
[13] L. Baker, L.C. Just, Studies of metals water reactions at high temperatures – III experimental and theoretical studies of the zirconium–water reaction, Technical Report ANL-6548, Argonne National Laboratory, May 1962.
[14] J.V. Cathcart, R.E. Pawel, Zirconium metal–water oxidation kinetics, IV Reaction Rate Studies, ORNL/NUREG-17.
[15] S. Leistikow, G. Schanz, Nucl. Eng. Des. 103 (1987) 65.
[16] A. Volchek, Yu. Zvonarev, G. Schanz, Nucl. Eng. Design 232 (1) (2004) 85.
[17] E.T. Hayes, A.H. Roberson, J. Electrochem. Soc. 96 (1949) 142.
[18] D.A. Powers, L.N. Kmetyk, R.C. Schmidt, A review of technical issues of air ingression during severe reactor accidents, NUREG/CR-6218, September 1994.
[19] M. Blat-Yrieix, A. Ambard, F. Foct, A. Miquet, N. Cayet, Toward a Better Understanding of Dimensional Changes in Zircaloy-4: What is the Impact Induced by Hydrides and Oxide Layer?, Zirconium in the Nuclear Industry, in: Fifteenth International Symposium, Sunriver Oregon, June 2007.
[20] Martin Steinbrück, Alexei Miassoedov, Gerhard Schanz, Leo Sepold, J. Nucl. Eng. Design 236 (14-16) (2006) 1709.
[21] L. Portier, T. Bredel, J.-C. Brachet, V. Maillot, J.-P. Mardon, A. Lesbros, M. Billone, B. Cox, A.T. Motta, Influence of long service exposures on the thermal-mechanical behaviour of Zy-4 and M5™ alloys in LOCA conditions, ASTM Special Technical Publication 1467, 2005, p. 896.
[22] Klepfer, cited in Fuel Cladding Embrittlement During a Loss-of-Coolant-Accident, G.J. Catena, NEDO 10674, General Electric Company, October 1972, 1968.
[23] E.C. Subbarao, in: A.H. Heuer, L.W. Hobbs (Eds.), Advances in Ceramics, Vol. 3, The American Ceramic Society, Columbus, 1981.
[24] B. Cox, Oxidation of zirconium and its alloys, in: M.G. Fontana, R.W. Staehle (Eds.), Advances in Corrosion Science and Technology, Vol. 5, Plenum Press, 1976.
[25] S. Leistikow, G. Schanz, High temperature oxidation of Zircaloy-4 cladding tubes in steam (600–1600 °C), Ninth International Meeting on Metallic Corrosion, Toronto, Canada, 3–7 June 1984.
[26] J.H. Baek, K.B. Park, Y.H. Jeong, J. Nucl. Mater. 335 (2004) 443.
[27] M. Steinbrück, U. Stegmaier, T. Ziegler, Prototypical experiments on air oxidation of Zircaloy-4 at high temperatures, FZK Report 7257, January 2007.
[28] T.J. Chung et al., J. Am. Ceram. Soc. 82 (11) (1999) 3193.
[29] T.J. Chung et al., J. Am. Ceram. Soc. 80 (10) (1997) 2607.
[30] Y. Chen, D.P. Tompson, J. Am. Ceram. Soc. 74 (5) (1991) 1135.